Received August 29, 2021, accepted September 10, 2021, date of publication September 14, 2021,
date of current version September 22, 2021.

Digital Object Identifier 10.1109/ACCESS.2021.3112771

Metasurface Cloaks to Decouple Closely Spaced Printed Dipole Antenna Arrays Fed by a Microstrip-to-Balanced Transmission-Line Transition

DOOJIN LEE[1], (Member, IEEE), AND ALEXANDER B. YAKOVLEV[2], (Senior Member, IEEE)
[1]Maritime Technology Research Institute, Agency for Defense Development, Jinhae 51678, Republic of Korea
[2]Department of Electrical and Computer Engineering, University of Mississippi, Oxford, MS 38677, USA

Corresponding author: Doojin Lee (djlee@add.re.kr)

ABSTRACT In this work, we present a numerical study of 1D and 2D closely spaced antenna arrays of microstrip dipole antennas covered by a metasurface in order to properly cloak and decouple the antenna arrays operating at neighboring frequencies. We show that the two strongly coupled arrays fed by a microstrip-to-balanced transmission-line transition are effectively decoupled in 1D and 2D array scenarios by covering the dipole antenna elements with an elliptically shaped metasurface. The metasurface comprises sub-wavelength periodic metallic strips printed on an elliptically shaped dielectric cover around the dipole antennas and integrated with the substrate. We present a practical design of cloaked printed dipole arrays placed in close proximity of each other and demonstrate that the arrays are decoupled in the near field and operate independently in the far field with their original radiation characteristics as if they were isolated.

INDEX TERMS Antenna arrays, beam steering, elliptical metasurface, mantle cloaks, microstrip-to-balanced transmission-line transition, mutual coupling, phased arrays.

I. INTRODUCTION

In recent years, there has been an increasing demand in the analysis, design, modeling, and practical realization of electromagnetic cloaks ranging from microwaves to optics. The cloaking/invisibility of an object is of great interest in military, communication, and industrial applications. For example, the reduced interference and low visibility of a receiving antenna in sensing, imaging, monitoring, and communication applications are typically required to improve the overall performance of the system and make the system robust, which is achieved by cloaking the receiving antenna [1]–[5]. The elimination of the mutual coupling between tightly arranged antenna elements is also one of the main applications utilizing the cloaking technique [1], [6]–[9].

The electromagnetic cloaks can be divided into two groups of cloaks based on guided-wave and scattering cancellation wave phenomena, respectively. The guided-wave cloaks include the transformation optics (TO) based cloaks and the transmission-line (TL) based cloaks. In the TO-based cloaks the electromagnetic waves bend around the object to be cloaked, which reduces the scattered field from the object and makes it invisible to an observer [10]–[12]. However, the TO-based cloaks utilize bulky metamaterials, and this creates difficulties in the practical realization and significantly increases the dielectric/conduction losses due to a volumetric metamaterial with dimensions comparable with the size of the object to be cloaked. The TL-based cloaks [13]–[15] utilize the electromagnetic coupling between the transition layer and the transmission-line network. This method is mainly useful for the reduction of interference from the blockage placed in front of the antenna [16]. On the other hand, the scattering cancellation cloaks include the plasmonic cloaking and metasurface cloaking techniques. The plasmonic cloaks [17]–[22] employ the negative dielectric permittivity of isotropic materials to eliminate the dominant scattering field, which is difficult to realize in practical applications [3], [19], [23], [24]. However, the metasurface-based cloaking technique, called a mantle cloaking, has recently gained much attention because of its low-profile design, which is realized by an ultra-thin

The associate editor coordinating the review of this manuscript and approving it for publication was Mohammed Bait-Suwailam.

surface of sub-wavelength periodic elements [1], [3], [7], [8], [25]–[29]. In the mantle cloaking the anti-phase surface currents are excited on the metasurface resulting in the scattering cancellation of the dominant scattering mode from the object to be cloaked [7], [8], [28]. A practical realization of metasurface cloaks and microwave measurements have been recently performed for dielectric and metallic cylindrical objects [25], [30]–[33] and with closely spaced antennas to reduce the mutual coupling between the antennas and restore their original radiation patterns [1], [34]–[37]. However, in these works the fabrication and microwave measurements have been performed for free-standing cylindrical objects and free-standing antennas, and the first attempt to integrate the metasurface cloaks with printed microstrip antennas has been done in [37] with 3D dielectric printers.

Mantle cloaks have several advantages, such as their flexibility in the design process, their invisibility for all angles of incidence, and the ease in the fabrication process, compared to the other methods. The mantle cloaks have been implemented to the narrowband [7], [8], [28] and even wideband cloaking applications [8], [15], [38]. Most work on the narrowband antenna applications, concerning the operation at the neighboring frequencies, have utilized the ultrathin metasurface-based cloaks to reduce the mutual coupling between the radiating elements, and at the same time, to preserve the antenna radiation pattern when placed in close proximity (i.e., $\lambda_0/10$, where λ_0 is the operating or design frequency of the antenna) [7], [28]. In [29], an analytical model for the electromagnetic scattering from the cylindrical dielectric or metallic object with an ultrathin metasurface, comprising 1D and 2D arrays of the sub-wavelength periodic elements, is fundamentally studied to investigate the reduction of the total scattering width at the design frequency. In [26], the scattering reduction from the dielectric/metallic cylinder is studied with the line-source excitation placed in close proximity to the cloaked object. The significant reduction of the scattering width for electromagnetic cloaking applications is also achieved at the low-terahertz frequencies by covering the cylindrical objects or antennas with the thinnest possible mantle cloak utilizing an atomic graphene sheet [27], [39]–[41]. The confocal elliptically shaped metasurface was proposed for strip-dipole antennas to reduce the mutual coupling and to preserve the antenna radiation patterns for two cloaked antennas placed in close proximity [7], [28]. In [8], the wideband cloaks, comprising strongly coupled I-shaped metasurfaces, were proposed to cloak and decouple the wideband strip and microstrip monopoles within their bands of operation. In [38], the non-Foster-based metasurface cloak was implemented to enlarge the bandwidth of operation in order to overcome the bandwidth limitations of the passive metasurface cloaks.

With the recent technological developments, the demand for high-density platforms with closely spaced radiating elements, such as multiple-input multiple-output (MIMO) antenna systems and multiple antenna arrays, has been highly increased in the areas of military, communication, and industrial applications [8], [42]. The interleaved antenna arrays within a limited physical space among the radiating elements are highly vulnerable to the electromagnetic interference and mutual coupling between the neighboring antenna elements. With the development of the mantle cloaking technique, these issues can be addressed. In this regard, in [42] the cloaking and decoupling of the tightly coupled antenna arrays was recently introduced with the use of elliptically shaped metasurface cloaks.

In this paper, we further extend the decoupling and cloaking approach to 1D and 2D arrays of printed dipoles fed by a microstrip-to-balanced transmission-line transition and with the metasurface cloaks integrated with printed technology. We present a practical design of cloaked arrays of printed dipoles placed in close proximity and operating at neighboring frequencies within the 20 GHz frequency band. This concerns the satellite communication applications in the Ka-band. We demonstrate for 1D and 2D phased array configurations that the mutual coupling strongly affects the matching and radiation characteristics of the arrays, and the presence of the cloaks decouples the arrays in the near field and restores their original radiation patterns in the far field, as if the arrays were isolated. The numerical analysis is performed with the CST Microwave Studio [43].

To better highlight the novelty of this work we have created a comparison Table 1 with the other cloaked strip/microstrip antenna designs available in the literature.

TABLE 1. Comparative analysis of the proposed designs of cloaked 1D and 2D phased antenna arrays with the other cloaked strip/ microstrip antenna designs available in the literature.

Ref.	Antenna type	Array	Cloaked frequency	Feed line	Metasurface structure	Analysis method
This work	Printed dipole	1D /2D printed array	20 / 22 GHz (narrow band)	Transition feed network	Thin metallic strip	Numerical analysis
[7]	Strip dipole	-	3/3.5GHz (narrow band)	Lumped port	Thin metallic strip	Analytical and numerical analyses
[8]	Strip monopole	-	2.5 /4.5 GHz/ 7 /16 GHz (wide band)	Strip line	I-shaped unit cells	Numerical analysis
[28]	Printed monopole	-	3/3.3 GHz (narrow band)	Strip line	Thin metallic strip	Numerical analysis
[39]	Strip dipole	-	1.86/2.59THz (narrow band)	Lumped port	Thin graphene monolayer	Numerical analysis
[42]	Strip monopole	1D strip array	2.95/3.35GHz (narrow band)	Lumped port	Thin metallic strip	Analytical and numerical analyses

This paper is organized as follows. In Section II, the single planar dipole antennas with and without the metasurface cloaks operating at neighboring frequencies within the 20 GHz band and fed by a microstrip-to-balanced transmission-line transition are presented, and the matching and radiation characteristics are investigated and discussed when two single planar dipole antennas are placed in close proximity of each other. With the mantle cloaking technique, the 1D and 2D arrays of printed dipoles, fed by the multi-port feed network, with steering the beam toward the certain angle

are numerically explored in Section III. The conclusions are drawn in Section IV.

II. SINGLE PRINTED PLANAR DIPOLE ANTENNA

In this section, we explore the antenna performance with and without the metasurface cloaks when two single printed planar dipole antennas are placed in close proximity. Two printed dipole antennas fed by a microstrip-to-balanced transmission-line transition are designed to operate at the neighboring frequencies of 20.5 GHz. The elliptically shaped metasurface, comprising thin metallic strips printed on an elliptically shaped dielectric cover around the antennas, is designed with the cloaking effect for the frequencies of antenna operation. The antenna characteristics, such as scattering parameters, radiation pattern, total efficiency, electric field distribution, and current distribution, are investigated with respect to the cloaked and uncloaked antenna sets when two printed planar dipole antennas are placed in close proximity of each other.

A. STAND-ALONE PLANAR DIPOLE ANTENNAS

First, the two printed planar dipole antennas are designed on both sides of the substrate using the CST Microwave Studio with the geometry shown in Fig. 1. The substrate (Rogers RT / duroid 5870) with 0.79 mm thickness is used with the dielectric constant of 2.33 and the loss tangent of 0.0005. The printed planar dipole antenna in this study is fed by the microstrip-to-balanced transmission-line transition, which not only transforms the impedance from 50 Ω to 188 Ω but also makes the end of the line balanced [44]–[46]. The balanced transmission line consists of the microstrip and parallel lines. The width of each transmission line can be easily determined by using a microstrip line equation, which can be found in [47]. The parallel strip-lines, which have the same widths with respect to the signal and ground lines, can be designed by implementing an image theory to the original equation of the microstrip line [44]–[46].

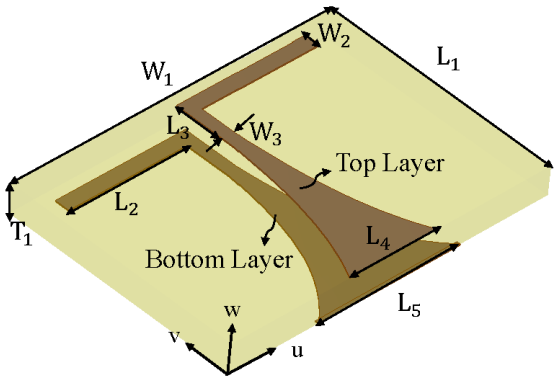

FIGURE 1. Single printed planar dipole antenna fed by a microstrip-to-balanced transmission-line transition. The top layer is printed on the top interface and the bottom layer is printed on the bottom interface of the substrate.

The antenna parameters, as shown in Fig. 1, are determined to reduce the mismatch loss: $W_1 = 9$ mm, $W_2 = 0.4$ mm, $W_3 = 0.33$ mm, $L_1 = 6.44$ mm, $L_3 = 1.64$ mm, $L_4 = 2.45$ mm, $L_5 = 4$ mm, $T_1 = 0.79$ mm, and $T_2 = 0.035$ mm. The lengths of the printed dipole 1 ($L_2 = 3.65$ mm) and dipole 2 ($L_2 = 3.5$ mm) are determined to resonate at the neighboring frequencies around 20 GHz and 21 GHz, respectively.

Figs. 2 (a)-(b) show the simulation results of the isolated uncloaked printed planar dipole antennas (original isolated antennas without the cloak). The antennas resonate at the neighboring frequencies as shown in Fig. 2(a) with the total efficiency around 80 % for both antennas (Fig. 2(b)).

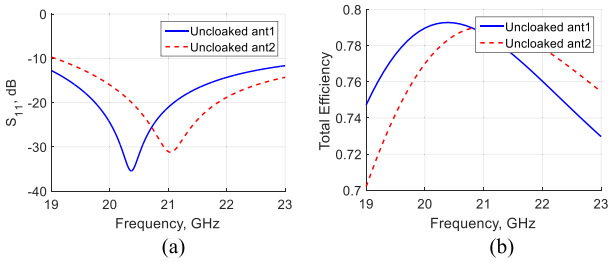

FIGURE 2. Characteristics of the isolated uncloaked printed planar dipole antennas; (a) Reflection coefficient, (b) Total efficiency.

Next, the cloaked printed planar dipole antennas are designed as shown in Figs. 3 (a)-(c). The thin metallic strips, as shown in Fig. 3 (c), are mounted on the elliptically shaped dielectric material with the goal to achieve the required surface reactance of the metasurface, resulting in the scattering cancellation of the dominant scattering mode from the object to be cloaked. In this work, the elliptically shaped metasurfaces are partially integrated with the substrate as shown in Fig. 3 (b). The parameters of the cloaked printed planar dipole antennas are the same as those of the isolated uncloaked (original) printed dipole antennas, except for the antenna length. The metasurfaces have the following parameters: the width (w) and periodicity (D) of the thin metallic strips, the focal point (F) of the metasurfaces at the edges of the strip dipole antenna, dielectric constant (ε_m), perimeter (P), and the major (a) and minor semi-axes (b) of the elliptically shaped dielectric material. The parameters are listed in Table 2.

TABLE 2. Design parameters of the printed cloaked antennas.

Cloaking parameters	Cloaked antenna 1	Cloaked antenna 2
Length, L_6	3.167 mm	3.167 mm
Dielectric constant, ε_m	5.667	6.556
Width of metallic strips, w	0.050 mm	0.050 mm
Periodicity, D	0.340 mm	0.340 mm
Perimeter, P	1.020 mm	1.020 mm
Focus, F	0.200 mm	0.200 mm
Major semi-axis, a	0.220 mm	0.220 mm
Minor semi-axis, b	0.092 mm	0.092 mm
Number of strips, N	6	6

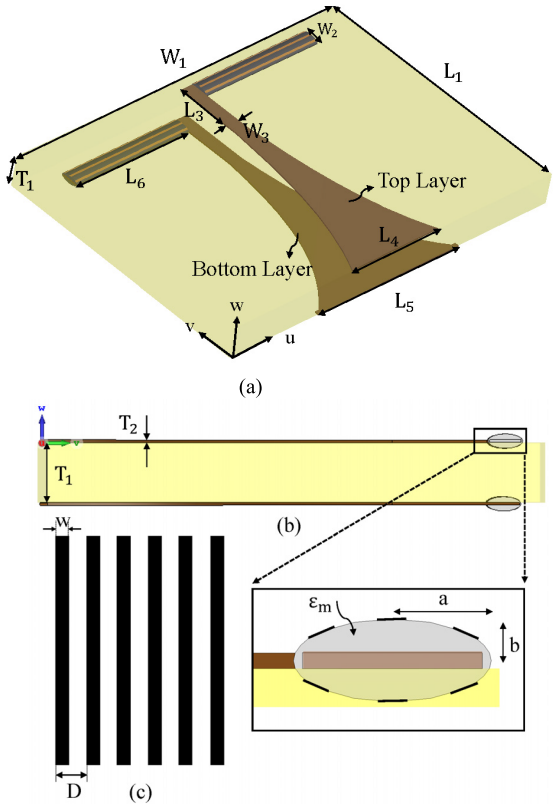

FIGURE 3. Single cloaked printed dipole antenna fed by a microstrip-to-balanced transmission-line transition; (a) 3D view; (b) VOW view; (c) Configuration of the thin metallic strips of the metasurface cloak.

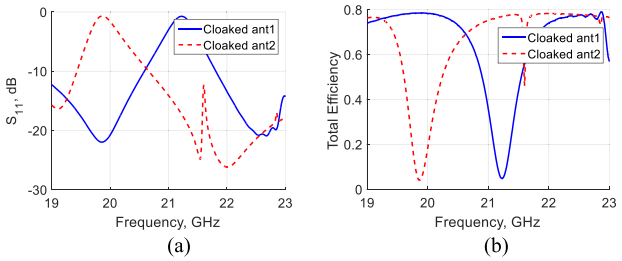

FIGURE 4. Characteristics of the cloaked printed planar dipole antennas; (a) Reflection coefficient, (b) Total efficiency.

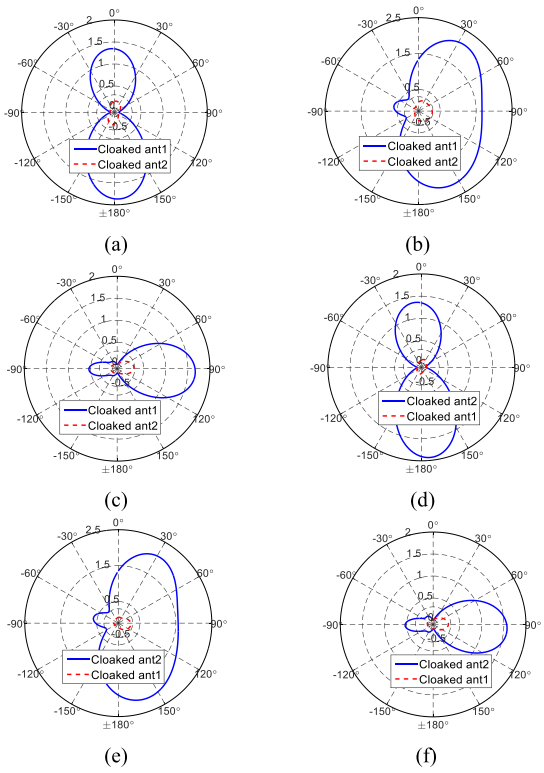

FIGURE 5. 2D linear radiation patterns of the cloaked printed planar dipole antennas at the corresponding frequencies; (a) UOW plane ($\phi = 0°$) at 19.8 GHz; (b) VOW plane ($\phi = 90°$) at 19.8 GHz; (c) UOV plane ($\theta = 90°$) at 19.8 GHz; (d) UOW plane ($\phi = 0°$) at 21.3 GHz; (e) VOW plane ($\phi = 90°$) at 21.3 GHz; (f) UOV plane ($\theta = 90°$) at 21.3 GHz.

Figs. 4 (a)-(b) show the reflection coefficient and the total efficiency against frequency, respectively. The cloaked printed planar antennas are specifically designed to resonate around 20 GHz (cloaked antenna 1), and at the same time, to cloak the neighboring antenna around 21 GHz (cloaked antenna 2) and vice versa. The combination of the inductive and capacitive components, which represent the surface reactance, can be adjusted by changing the width and periodicity of the thin metallic strips. The dielectric constant of the elliptically shaped dielectric material is also a key parameter to determine the surface reactance to reduce the dominant scattering energy from the object. The total efficiency of the cloaked antennas around 80 %, which is very close to that of the total efficiency of the isolated uncloaked (original) antennas, is obtained at the designed frequency.

Figs. 5 (a)-(f) show the 2D linear radiation patterns of the cloaked printed planar antennas. The radiation patterns are obtained at 19.8 GHz for the cloaked antenna 1 and 20.3 GHz for the cloaked antenna 2. Unlike the uncloaked printed planar dipole antennas, the radiation patterns of the cloaked antennas show poor radiation at the frequency to be cloaked. This is because the designed metasurfaces effectively cancel the scattered field of the antenna to be cloaked.

In Figs. 6 (a)-(d) the electric-field distribution of the incident transverse magnetic (TM) plane wave is shown in the presence of the cloaked antennas 1 and 2 at the corresponding frequencies. The electric field is severely distorted for the cloaked antenna 1 at 19.8 GHz (Fig. 6 (a)) and for the cloaked antenna 2 at 21.3 GHz (Fig. 6 (d)) due to the strong scattered field. However, the electric field is nearly uniform as shown in Fig. 6 (b) for the cloaked antenna 1 at 21.3 GHz and as shown in Fig. 6 (c) for the cloaked antenna 2 at 19.8 GHz, which is effectively cloaked.

B. COUPLED PLANAR DIPOLE ANTENNAS

In this section, we explore the mutual coupling and the electromagnetic radiation of the antennas with and without the mantle cloaks when two printed planar dipole antennas are placed in close proximity of each other. Here, we investigate the mutual coupling between the two antennas operating at

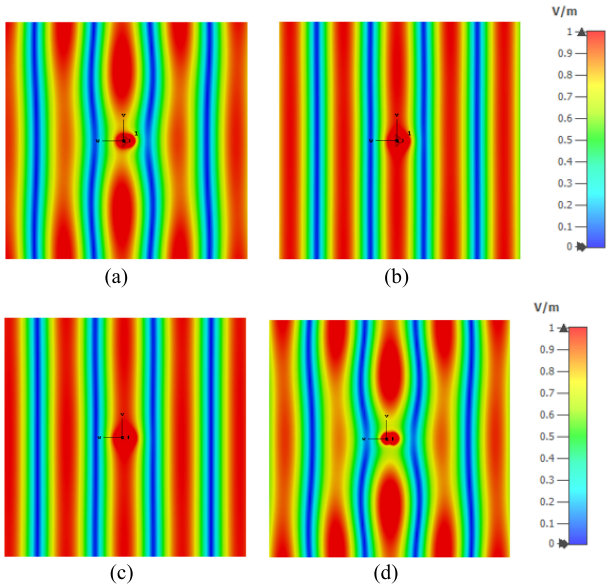

FIGURE 6. Electric-field distribution of the cloaked antennas; (a) Cloaked antenna 1 at 19.8 GHz; (b) Cloaked antenna 1 at 21.3 GHz; (c) Cloaked antenna 2 at 19.8 GHz; (d) Cloaked antenna 2 at 21.3 GHz.

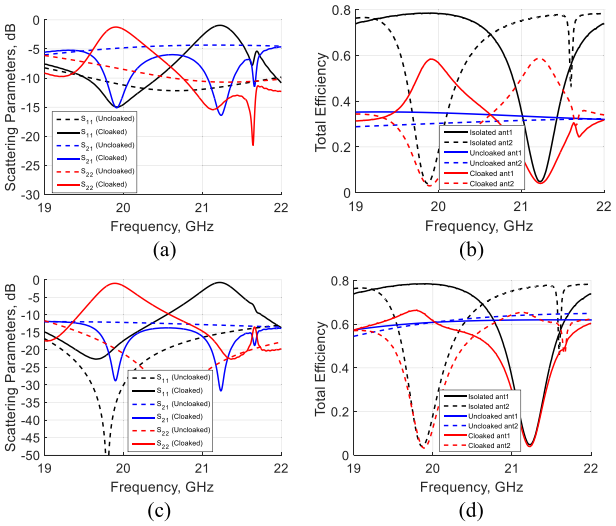

FIGURE 7. Characteristics of the coupled printed planar dipole antennas; (a) Scattering parameters at the distance of $\lambda_0/15$; (b) Total efficiency at the distance of $\lambda_0/15$; (c) Scattering parameters at the distance of $\lambda_0/3$; (d) Total efficiency at the distance of $\lambda_0/3$.

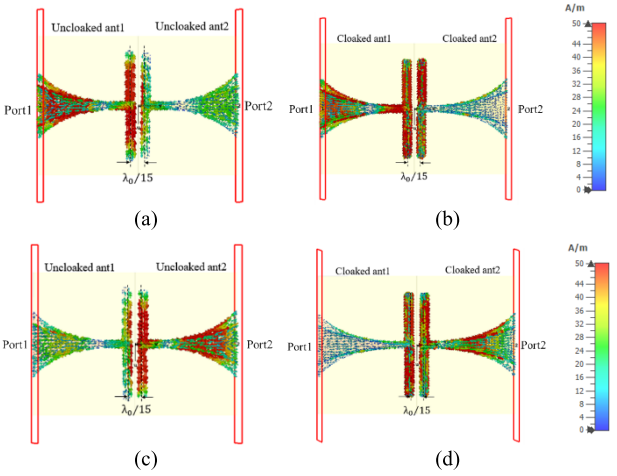

FIGURE 8. Current distribution of the closely spaced printed planar dipole antennas with the same dynamic ranges; (a) Uncloaked coupled planar dipole antennas at 19.8 GHz; (b) Cloaked coupled planar dipole antennas at 19.8 GHz; (c) Uncloaked coupled planar dipole antennas at 21.3 GHz; (d) Cloaked coupled planar dipole antennas at 21.3 GHz.

the neighboring frequencies by placing the antennas at the distances of $\lambda_0/15$ and $\lambda_0/3$, where λ_0 is the free-space wavelength at 20.5 GHz. Figs. 7 (a)-(b) show the scattering parameters and the total efficiency when two planar dipole antennas are strongly coupled. It can be clearly seen in Fig. 7 (a) that the strong coupling less than -5 dB is observed for the uncloaked planar dipole antennas, whereas the mutual coupling is significantly reduced to more than -15 dB around 20 GHz and 21 GHz for the cloaked planar dipole antennas. The corresponding total efficiency results demonstrate that approximately half of the total efficiency is reduced for the uncloaked case due to strong mutual coupling, while the total efficiency of approximately 75 % is obtained for the cloaked case when two planar dipole antennas are placed at the distance of $\lambda_0/15$. We further explore the scattering parameters (Fig. 7 (c)) and the total efficiency (Fig. 7 (d)) by increasing the distance between the antennas to $\lambda_0/3$. The coupling level of the uncloaked and cloaked cases is around -12 dB and -30 dB, respectively. The total efficiency of the cloaked planar dipole antennas is around 82 % at 19.8 GHz (21.3 GHz), while the total efficiency is dramatically reduced to 5 % at 21.3 GHz (19.8 GHz).

The mutual coupling is also explored by the current distribution of the coupled printed planar dipole antennas as shown in Figs. 8 (a)-(d). The two printed planar dipole antennas are closely spaced at a distance of $\lambda_0/15$ for both uncloaked and cloaked cases. The port 1 is excited, and the current flow toward the port 2 is investigated and vice versa. The current flow from the port 1 to port 2 and the current distribution with the same dynamic range are studied at 19. 8 GHz for the uncloaked and cloaked cases as shown in Figs. 8 (a) and (b), respectively. It can be clearly seen that the current from the port 1 is hardly delivered to the port 2 for the cloaked case compared to the uncloaked case. This observation is also confirmed, as shown in Figs. 8 (c)-(d), in such a way that the only port 2 is excited and the current flow toward the port 1 is explored. The high intensity of the surface current on the metasurfaces is also observed for both cloaked cases, which cancels the dominant scattered field from the antenna to be cloaked.

The radiation patterns are then investigated when two antennas are placed in close proximity. Here, the radiation patterns of the uncloaked coupled and cloaked coupled antennas are compared with those for the isolated antennas at the distances of $\lambda_0/15$ and $\lambda_0/3$ to explore the effect of the mutual coupling on the radiation patterns as shown in Figs. 9 (a)-(f). The radiation patterns of the cloaked coupled antennas seem

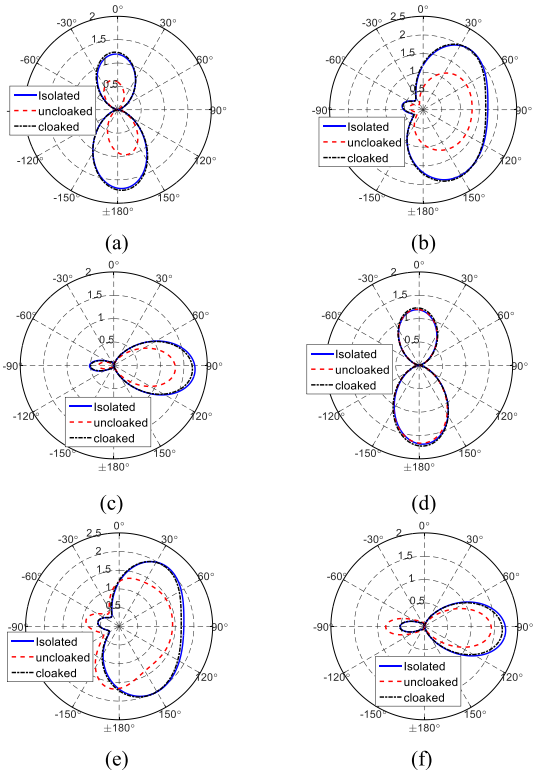

FIGURE 9. 2D linear radiation patterns of the isolated, uncloaked coupled, and cloaked coupled antennas at 19.3 GHz; (a) UOW plane ($\phi = 0°$) at the distance of $\lambda_0/15$; (b) VOW plane ($\phi = 90°$) at the distance of $\lambda_0/15$; (c) UOV plane ($\theta = 90°$) at the distance of $\lambda_0/15$; (d) UOW plane ($\phi = 0°$) at the distance of $\lambda_0/3$; (e) VOW plane ($\phi = 90°$) at the distance of $\lambda_0/3$; (f) UOV plane ($\theta = 90°$) at the distance of $\lambda_0/3$.

to be very close to those of the isolated antennas, while the patterns are severely distorted for the uncloaked coupled antennas for all the cut-planes. The metasurface-based cloaks restore the original radiation patterns of the antennas even for a deeply sub-wavelength separation of the antennas.

III. PRINTED PLANAR DIPOLE ANTENNA ARRAYS

We have investigated the matching and radiation characteristics of single printed planar dipole antennas with and without the metasurface cloaks and have demonstrated that the mutual coupling of the antennas placed in close proximity can be dramatically reduced with the metasurface cloaks, and the radiation patterns of the strongly coupled antennas can be restored as if the antennas were isolated. In this section, we further extend the study to explore the decoupling and cloaking effects in the printed arrays by comparing the results with and without the mantle cloaks for 1D and 2D antenna arrays with the beam steering toward a specific angle.

The 8 by 1 microstrip-to-balanced transmission-line network is proposed to properly feed each antenna element (Fig. 10). The feed network is designed to have approximately equal amplitude and phase among the ports so that the power is evenly distributed to each port. Each length and width of the parallel strip line is determined to operate around 20 GHz and optimized by the CST MWS. Each parameter of the lines is listed in Table 3.

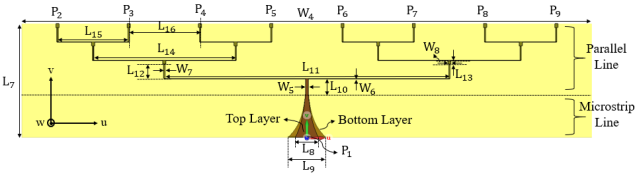

FIGURE 10. Proposed 8 by 1 microstrip-to-balanced transmission-line feed network.

TABLE 3. Parameters of the 8 by 1 microstrip-to-balanced transmission-line feed network.

L_7	13.30 mm	L_{14}	14.96 mm
L_8	2.45 mm	L_{15}	7.46 mm
L_9	4.00 mm	L_{16}	7.46 mm
L_{10}	1.60 mm	W_4	60.00 mm
L_{11}	29.96 mm	W_5	0.33 mm
L_{12}	1.88 mm	W_6	0.04 mm
L_{13}	0.36 mm	W_7	0.14 mm

The performance of the feed network is numerically evaluated by the scattering parameters and the phase difference as shown in Figs. 11 (a)-(b) for each port. The transmission coefficient level for each port, as shown in Fig. 11 (a), is about −10 dB, which is due to a 3 dB loss for each branch together with the surface leakage current and the loss tangent of the substrate. The phase difference is also investigated by subtracting the phase of the port 2 from each phase. The phase difference for the port 2, port 3, port 4, and port 5 is included here, as shown in Fig. 11 (b), as the feed network has a symmetric structure with respect to the VOW plane. It is shown to be around ± 1.5 degrees difference around 20 GHz, which is within an acceptable level.

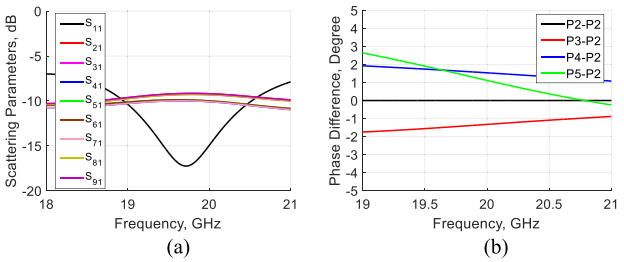

FIGURE 11. Performance of the proposed 8 by 1 feed network; (a) Scattering parameters; (b) Phase difference for each port.

A. 1D PLANNAR ARRAYS FED BY THE 8 BY 1 FEED NETWORK

The single cloaked antenna is laterally arranged to configure the 1D array as shown in Fig. 12. Every single antenna is spaced by the distance of $\lambda_0/2$, where λ_0 is the free-space wavelength at 20 GHz to avoid the grating lobes. The printed cloaked antennas are equally fed by the transmission-line transition network, which transforms the port impedance of 50 Ω to input impedance of 188 Ω at each port. The

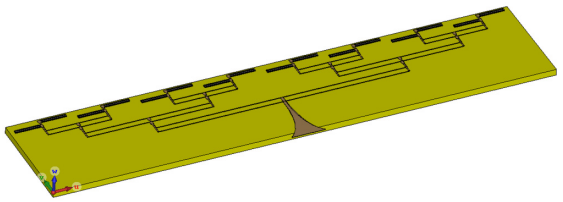

FIGURE 12. 1D printed planar dipole array fed by the microstrip-to-balanced transmission-line transition network.

antenna length and the dielectric constant of the dielectric cover of the cloaks are adjusted to operate the antennas around 20 GHz. The 1D array fed by the transition network is numerically evaluated by the scattering parameters and the total efficiency as shown in Fig. 13. The cloaked antenna array 1 resonates around 19.5 GHz and at the same time, the antenna array 1 cloaks the radiation of the array 2 around 20.2 GHz, where the cloaked antenna array 2 resonates as shown in Fig. 13 (a). The corresponding characteristic is also closely related to the total efficiency against the frequency as shown in Fig. 13 (b). The total efficiency of the cloaked antennas reaches its peak around 90 % at its resonant frequency.

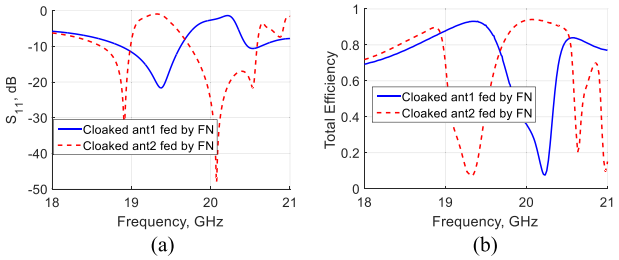

FIGURE 13. Performance of the 1D printed cloaked antenna arrays fed by the feed network (FN) against frequency; (a) Scattering parameters; (b) Total efficiency.

The 2D linear radiation patterns of the 1D printed cloaked antennas are explored as shown in Figs. 14 (a)-(f). The radiation patterns of the cloaked arrays are investigated in such a way that the patterns of the cloaked antenna arrays are explored around their resonant frequencies and at the same time the patterns of the arrays are also explored around the frequencies to be cloaked. It is clearly seen that the patterns of the cloaked arrays at the frequency to be cloaked show poor radiation. This is because the metasurface plays a key role to effectively cancel the scattered field from the array to be cloaked.

We investigated the characteristics of the 1D planar coupled antenna arrays at the very close distance, such as $\lambda_0/15$, as shown in Figs. 15 (a)-(b), to explore the mutual coupling and the total efficiency when two coupled arrays are placed in close proximity of each other. Each characteristic of the cloaked coupled planar arrays, such as the scattering parameters and the total efficiency against frequency, is compared with the uncloaked coupled arrays. As expected, the very strong mutual coupling is observed for the uncloaked coupled

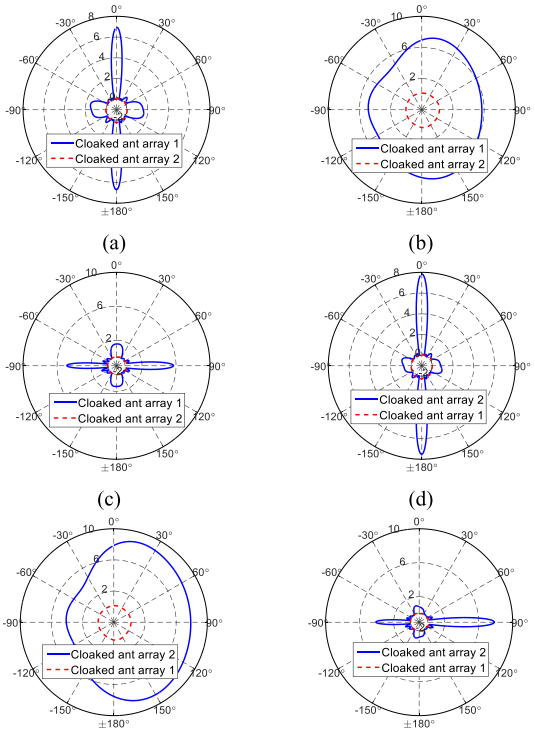

FIGURE 14. 2D linear radiation patterns of the cloaked printed planar antenna arrays at the corresponding frequencies; (a) UOW plane ($\phi = 0°$) at 19.5 GHz; (b) VOW plane ($\phi = 90°$) at 19.5 GHz; (c) UOV plane ($\theta = 90°$) at 19.5 GHz; (d) UOW plane ($\phi = 0°$) at 20.2 GHz; (e) VOW plane ($\phi = 90°$) at 20.2 GHz; (f) UOV plane ($\theta = 90°$) at 20.2 GHz.

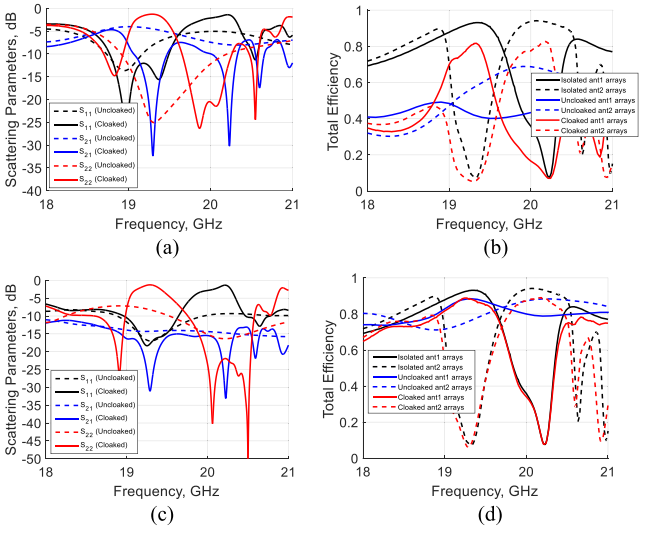

FIGURE 15. Characteristics of the coupled printed planar dipole antenna arrays; (a) Scattering parameters at the distance of $\lambda_0/15$; (b) Total efficiency at the distance of $\lambda_0/15$; (c) Scattering parameters at the distance of $\lambda_0/3$; (d) Total efficiency at the distance of $\lambda_0/3$.

arrays whereas the mutual coupling is significantly reduced around 19.3 GHz and 20.2 GHz for the cloaked coupled arrays, showing the transmission coefficient (S21) level of more than −30 dB (Fig. 15 (a)). The corresponding total efficiency is shown in Fig. 15 (b), demonstrating that it

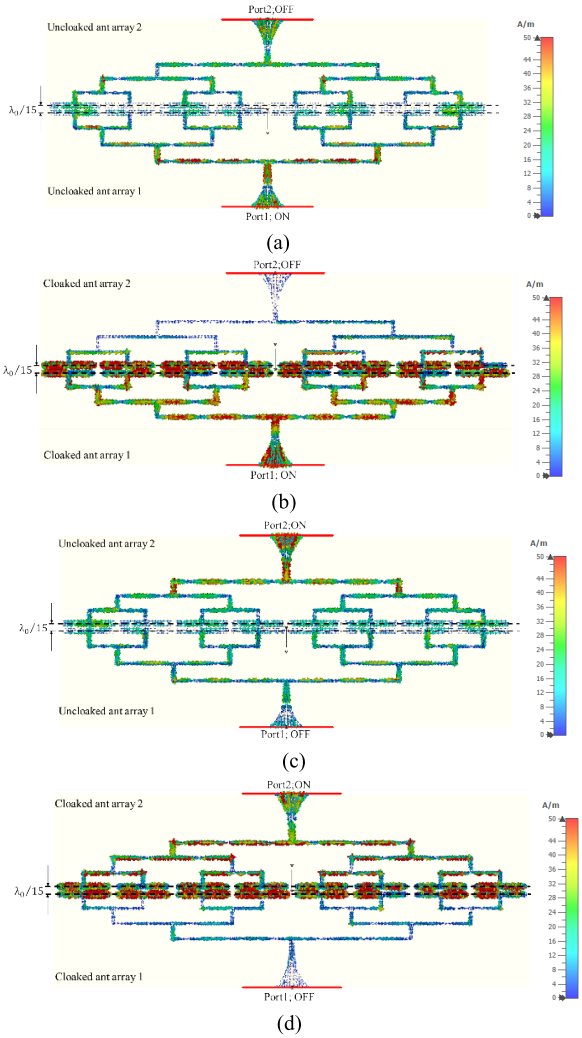

FIGURE 16. Current distribution of the closely spaced printed planar arrays with the same dynamic ranges; (a) Uncloaked coupled arrays at 19.3 GHz; (b) Cloaked coupled arrays at 19.3 GHz; (c) Uncloaked coupled arrays at 20.2 GHz; (d) Cloaked coupled arrays at 20.2 GHz.

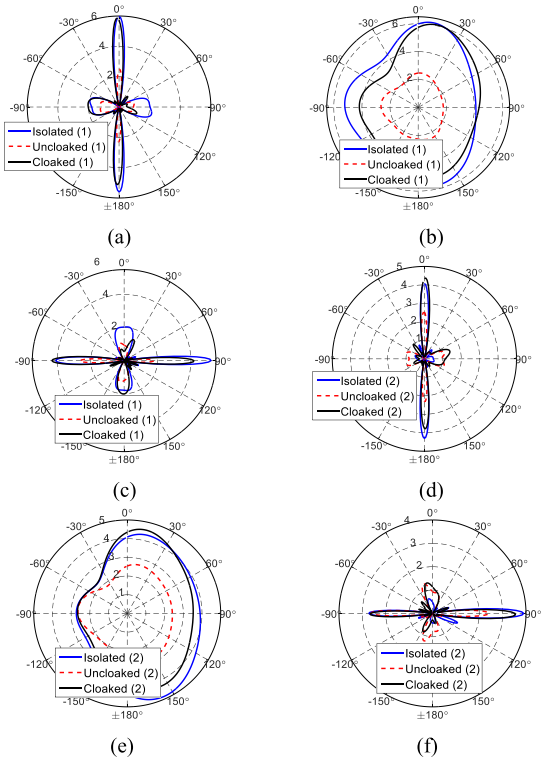

FIGURE 17. 2D linear radiation patterns of the isolated, uncloaked, and cloaked coupled arrays at the distance of $\lambda_0/15$; (a) UOW plane ($\phi = 0°$) at 19.8 GHz; (b) VOW plane ($\phi = 90°$) at 19.8 GHz; (c) UOV plane ($\theta = 90°$) at 19.8 GHz; (d) UOW plane ($\phi = 0°$) at 20.6 GHz; (e) VOW plane ($\phi = 90°$) at 20.6 GHz; (f) UOV plane ($\theta = 90°$) at 20.6 GHz.

reaches up to 81% for the cloaked coupled arrays, and reduces to 5 % at the frequency to be cloaked. We further explore this study by increasing the distance between the two arrays to $\lambda_0/3$, as shown in Figs. 15 (c)-(d). It can be numerically confirmed that the decoupling between two closely spaced arrays is observed for the cloaked coupled arrays as shown in Fig. 15 (c) and the total efficiency reaches its maximum value comparable to that of the isolated arrays as shown in Fig. 15 (d).

Figs. 16 (a)-(d) show the current distribution of the coupled planar arrays for the case when two arrays are placed with a deeply sub-wavelength separation of $\lambda_0/15$. Here, we explore the current distribution in such a way that the only port 1 is turned on and at the same time the current distribution is investigated at the port 2 and vice versa. The current from the port 1 at 19. 3 GHz, as shown in Fig. 16 (a), is delivered to the port 2 for the uncloaked coupled array due to the strong coupling. However, the current from the port 1, as shown in Fig. 16 (b), is hardly delivered to the port 2 for the cloaked coupled arrays. This is because the metasurface properly cloaks the array at the cloaking frequency and decouples the array ports. In a similar way, the current distribution is explored at the port 1 when only the port 2 is excited for the uncloaked and cloaked coupled arrays as shown in Figs 16. (c)-(d). For both cloaked coupled arrays as shown in Fig. 16 (b) and (d), the strong surface current is observed on the metasurface as expected.

The 2D linear realized gain of the coupled printed planar arrays is then explored on the cut planes as shown in Figs. 17 (a)-(f). The radiation patterns of the isolated, uncloaked, and cloaked cases are investigated in such a way that the strip dipole antenna array (without the feed network to avoid any radiation distortion from the feed network) is presented in front of the printed planar dipole array (with the feed network) at the distance of $\lambda_0/15$. The radiation patterns are then explored at the port 1 around 19.8 GHz as shown in Figs. 17 (a)-(c), whereas the patterns are investigated at the port 2 around 20.6 GHz as shown in Figs. 17 (d)-(f). The radiation patterns of the uncloaked coupled arrays are severely affected by the presence of the uncloaked antenna array leading to the distortion of the patterns. However, the radiation patterns of the cloaked coupled arrays are close to those of the isolated arrays due to the cloaking effect.

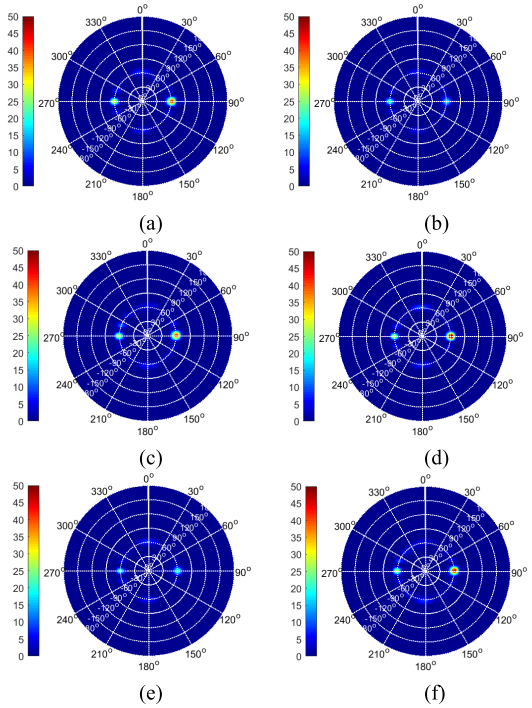

FIGURE 18. 3D linear realized gain plot with the beam steering toward the 30 degrees for the 2D coupled arrays at the distance of $\lambda_0/15$; (a) Isolated 2D array at 19.6 GHz; (b) Uncloaked coupled 2D array at 19.6 GHz; (c) Cloaked coupled 2D array at 19.6 GHz; (d) Isolated 2D array at 20.5 GHz; (e) Uncloaked coupled 2D array at 20.5 GHz; (f) Cloaked coupled 2D array at 20.5 GHz.

B. 2D PLANNAR ARRAYS FED BY THE 8 BY 8 FEED NETWORK

In this section, we further explore the array study for 2D coupled arrays, with steering the beam toward a specific angle, arranged as a stack of longitudinal 1D arrays discussed in the previous section. Here, the eight longitudinal configurations are made by placing each 1D array set at the distance of $\lambda_0/2$, where λ_0 is the wavelength at 20 GHz. Each 1D array has an equal amplitude and progressive phase shift to steer the beam toward the specific angle.

Figs. 18 (a)-(f) show the 3D linear gain plot for the 2D coupled arrays. We explore the radiation patterns of the 2D coupled arrays for the cases of isolated, uncloaked, and cloaked arrays in such a way that the 2D printed planar array (with the feed network) is coupled to the 2D dipole array (without the feed network to avoid any radiation distortion from the feed network) at the close distance of $\lambda_0/15$, and at the same time the patterns with the beam steering toward the 30 degrees are explored with the 3D plots. Here, the 3D plots include the three cut planes, such as UOW plane ($\phi = 0°$), VOW plane ($\phi = 90°$), UOV plane ($\theta = 90°$) and the intensity of the pattern. The angle ϕ is varied from 0 to 360 degrees with the 30 degrees interval, while the angle θ is varied from -180 to 180 degrees with the 30 degrees interval. The radiation pattern of the 2D printed array 1 is investigated at 19.6 GHz, which is coupled to the 2D strip array as shown in Figs. 18 (a)-(c), whereas the pattern of the 2D printed array 2 is explored at 20.5 GHz as shown in Fig. 18 (d)-(f), including the pattern of the isolated printed 2D array for the comparison. It is clearly seen that the patterns of the 2D cloaked coupled arrays are close to the patterns of the isolated 2D arrays with the main beam steered toward the 30 degrees. Note that the ϕ and θ angles of the boresight of the beam are originally at 90 and 90 degrees, respectively. However, the intensity of the 2D uncloaked coupled arrays is lower than the intensity of the isolated or cloaked cases, which is due to the strong mutual coupling between the arrays.

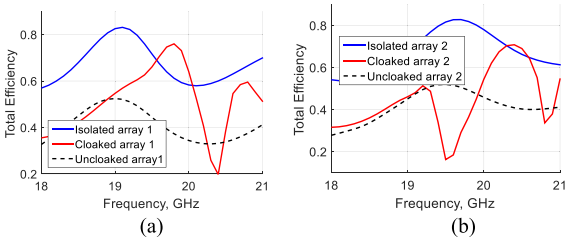

FIGURE 19. Total efficiency of the 2D coupled arrays at the distance of $\lambda_0/15$; (a) Total efficiency of the coupled antenna array 1; (b) Total efficiency of the coupled antenna array 2.

Figs. 19 (a)-(b) show the total efficiency against frequency when the 2D printed coupled arrays are placed at the close distance of $\lambda_0/15$. The total efficiency of the 2D uncloaked and cloaked arrays is investigated and compared with the total efficiency of the 2D isolated array. The total efficiency of the cloaked coupled arrays is approximately 70 % at 19.6 GHz as shown in Fig. 19 (a) and at 20.5 GHz as shown in Fig. 19 (b). Unlike the cloaked coupled cases, the total efficiency of the uncloaked coupled arrays is approximately 40 %, which is a relatively low value compared to the isolated or cloaked coupled cases. This is because the energy is strongly coupled between the two arrays. However, the cloaked coupled arrays effectively decouple each other at the frequency to be cloaked. This can be confirmed by the total efficiency of approximately 20 % at 20.5 GHz as shown in Fig. 19 (a) and at 19.6 GHz as shown in Fig. 19 (b).

IV. CONCLUSION

In this paper, we have proposed to apply the mantle cloaking technique to 1D and 2D printed dipole arrays operating at the neighboring frequencies and fed by the 8 by 1 feed network for the 1D array and 8 by 8 feed network for the 2D array. A single printed dipole antenna coated with an ultra-thin elliptically shaped metasurface has been designed with the practical microstrip-to-balanced transmission-line transition. It was numerically confirmed with the CST MWS numerical simulations that the metasurface cloaks integrated in printed technology made two tightly coupled antennas to be effectively decoupled and cloaked with the matching and radiation characteristics restored as if the antennas were isolated. It was also shown that the metasurface cloaks drastically reduce the mutual coupling between two phased antenna arrays in 1D and 2D configurations placed in close proximity of each

other, such that the cloaked arrays operate independently with their original radiation patterns. The fabrication and practical realization of the printed cloaked arrays is currently in progress, which requires a development of a 3D printed technology in order to integrate the metasurface cloaks with printed antennas and arrays. This technology has not been developed yet, and to the best of our knowledge in order to integrate metasurface cloaks with printed antennas the fully automated 3D metal-dielectric printers are required. This is the next step in the 3D fabrication of the proposed cloaked printed arrays and to perform the near-field and far-field microwave measurements.

REFERENCES

[1] J. C. Soric, A. Monti, A. Toscano, F. Bilotti, and A. Alù, "Dual-polarized reduction of dipole antenna blockage using mantle cloaks," *IEEE Trans. Antennas Propag.*, vol. 63, no. 11, pp. 4827–4834, Nov. 2015.
[2] J. B. Andersen and A. Frandsen, "Absorption efficiency of receiving antennas," *IEEE Trans. Antennas Propag.*, vol. 53, no. 9, pp. 289–2843, Sep. 2005.
[3] J. C. Soric, R. Fleury, A. Monti, A. Toscano, F. Bilotti, and A. Alù, "Controlling scattering and absorption with metamaterial covers," *IEEE Trans. Antennas Propag.*, vol. 62, no. 8, pp. 4220–4229, Aug. 2014.
[4] A. Alù and N. Engheta, "Cloaking a sensor," *Phys. Rev. Lett.*, vol. 102, Jun. 2009, Art. no. 233901.
[5] R. Fleury, J. Soric, and A. Alù, "Physical bounds on absorption and scattering for cloaked sensors," *Phys. Rev. B, Condens. Matter*, vol. 89, no. 4, 2014, Art. no. 045122.
[6] A. Monti, J. Soric, A. Alù, F. Bilotti, A. Toscano, and L. Vegni, "Overcoming mutual blockage between neighboring dipole antennas using a low-profile patterned metasurface," *IEEE Antennas Wireless Propag. Lett.*, vol. 11, pp. 1414–1417, Dec. 2012.
[7] H. M. Bernety and A. B. Yakovlev, "Reduction of mutual coupling between neighboring strip dipole antennas using confocal elliptical metasurface cloaks," *IEEE Trans. Antennas Propag.*, vol. 63, no. 4, pp. 1554–1563, Apr. 2015.
[8] G. Moreno, A. B. Yakovlev, H. M. Bernety, D. H. Werner, H. Xin, A. Monti, F. Bilotti, and A. Alu, "Wideband elliptical metasurface cloaks in printed antenna technology," *IEEE Trans. Antennas Propag.*, vol. 66, no. 7, pp. 3512–3525, Jul. 2018.
[9] S. Velucci, A. Monti, M. Barbuto, A. Toscano, and F. Bilotti, "Progress and perspective on advanced cloaking metasurfaces: From invisibility to intelligent antennas," *EPJ Appl. Metamater.*, vol. 8, no. 7, pp. 1–19, 2021.
[10] D.-H. Kwon and D. H. Werner, "Restoration of antenna parameters in scattering environments using electromagnetic cloaking," *Appl. Phys. Lett.*, vol. 92, no. 11, Mar. 2008, Art. no. 113507.
[11] J. B. Pendry, D. Schurig, and D. R. Smith, "Controlling electromagnetic fields," *Science*, vol. 312, pp. 1780–1782, Jun. 2006.
[12] J. Li and J. B. Pendry, "Hiding under the carpet: A new strategy for cloaking," *Phys. Rev. Lett.*, vol. 101, Nov. 2008, Art. no. 203901.
[13] J. Vehmas, P. Alitalo, and S. A. Tretyakov, "Experimental demonstration of antenna blockage reduction with a transmission-line cloak," *IET Microw., Antennas Propag.*, vol. 6, no. 7, pp. 830–834, May 2012.
[14] P. Alitalo, O. Luukkonen, L. Jylha, J. Venermo, and S. A. Tretyakov, "Transmission-line networks cloaking objects from electromagnetic fields," *IEEE Trans. Antennas. Propag.*, vol. 56, no. 2, pp. 416–424, Feb. 2008.
[15] S. Tretyakov, P. Alitalo, O. Luukkonen, and C. Simovski, "Broadband electromagnetic cloaking of long cylindrical objects," *Phys. Rev. Lett.*, vol. 103, Sep. 2009, Art. no. 103905.
[16] P. Alitalo, J. Vehmas, and S. A. Tretyakov, "Reduction of antenna blockage with a transmission-like cloak," in *Proc. 5th Eur. Conf. Antennas Propag. (EuCAP)*, 2011, pp. 2399–2402.
[17] A. Alù and N. Engheta, "Achieving transparency with plasmonic and metamaterial coatings," *Phys. Rev. E, Stat. Phys. Plasmas Fluids Relat. Interdiscip. Top.*, vol. 72, no. 1, Jul. 2005, Art. no. 016623.
[18] W. Cai, U. K. Chettiar, A. V. Kildishev, and V. M. Shalaev, "Optical cloaking with metamaterials," *Nature Photon.*, vol. 1, no. 4, pp. 224–227, Apr. 2007.
[19] F. Bilotti, S. Tricarico, and L. Vegni, "Plasmonic metamaterial cloaking at optical frequencies," *IEEE Trans. Nanotechnol.*, vol. 9, no. 1, pp. 55–61, Jan. 2010.
[20] A. Alù and N. Engheta, "Cloaking a receiving antenna or a sensor with plasmonic metamaterials," *Metamaterials*, vol. 4, nos. 2–3, pp. 153–159, Aug. 2010.
[21] A. Monti, A. Alù, A. Toscano, and F. Bilotti, "Optical invisibility through metasurfaces made of plasmonic nanoparticles," *J. Appl. Phys.*, vol. 117, no. 12, Mar. 2015, Art. no. 123103.
[22] M. Fruhnert, A. Monti, I. Fernandez-Corbaton, A. Alù, A. Toscano, F. Bilotti, and C. Rockstuhl, "Tunable scattering cancellation cloak with plasmonic ellipsoids in the visible," 2016, *arXiv:1605.09231*. [Online]. Available: http://arxiv.org/abs/1605.09231
[23] A. Monti, F. Bilotti, and A. Toscano, "Optical cloaking of cylindrical objects by using covers made of core-shell nanoparticles," *IEEE Trans. Nanotech.*, vol. 9, no. 1, pp. 55–61, Dec. 2010.
[24] A. Monti, F. Bilotti, A. Toscano, and L. Vegni, "Possible implementation of epsilon-near-zero metamaterials working at optical frequencies," *Opt. Commun.*, vol. 285, pp. 3412–3418, Jul. 2012.
[25] J. C. Soric, P. Y. Chen, A. Kerkhoff, D. Rainwater, K. Melin, and A. Alù, "Demonstration of an ultralow profile cloak for scattering suppression of a finite-length rod in free space," *New J. Phys.*, vol. 15, no. 3, 2013, Art. no. 033037.
[26] Y. R. Padooru, A. B. Yakovlev, P.-Y. Chen, and A. Alù, "Line-source excitation of realistic conformal metasurface cloaks," *J. Appl. Phys.*, vol. 112, no. 10, Nov. 2012, Art. no. 104902.
[27] A. Forouzmand and A. B. Yakovlev, "Electromagnetic cloaking of a finite conducting wedge with a nanostructured graphene metasurface," *IEEE Trans. Antennas Propag.*, vol. 63, no. 5, pp. 2191–2202, May 2015.
[28] H. M. Bernety and A. B. Yakovlev, "Decoupling antennas in printed technology using elliptical metasurface cloaks," *J. Appl. Phys.*, vol. 119, Apr. 2016, Art. no. 014904.
[29] Y. R. Padooru, A. B. Yakovlev, P.-Y. Chen, and A. Alù, "Analytical modeling of conformal mantle cloaks for cylindrical objects using subwavelength printed and slotted arrays," *J. Appl. Phys.*, vol. 112, no. 3, Aug. 2012, Art. no. 034907.
[30] R. S. Schofield, J. C. Soric, D. Rainwater, A. Kerkhoff, and A. Alù, "Scattering suppression and wideband tunability of a flexible mantle cloak for finite-length conducting rods," *New J. Phys.*, vol. 16, no. 6, Jun. 2014, Art. no. 063063.
[31] A. Monti, J. C. Soric, A. Alù, A. Toscano, and F. Bilotti, "Anisotropic mantle cloaks for TM and TE scattering reduction," *IEEE Trans. Antennas Propag.*, vol. 63, no. 4, pp. 1775–1788, Apr. 2015.
[32] T. V. Teperik, S. N. Burokur, A. de Lustrac, G. Sabanowski, and G.-P. Piau, "Experimental validation of an ultra-thin metasurface cloak for hiding a metallic obstacle from an antenna radiation at low frequencies," *Appl. Phys. Lett.*, vol. 111, Jul. 2017, Art. no. 054105.
[33] P. Yuste, J. M. Rius, J. Romeu, S. Blanch, A. Heldring, and E. Ubeda, "A microwave invisibility cloak: The design, simulation, and measurement of a simple and effective frequency-selective surface-based mantle cloak," *IEEE Antennas Propag. Mag.*, vol. 60, no. 4, pp. 49–59, Aug. 2018.
[34] Z. H. Jiang, P. E. Sieber, L. Kang, and D. H. Werner, "Restoring intrinsic properties of electromagnetic radiators using ultralightweight integrated metasurface cloaks," *Adv. Funct. Mater.*, vol. 25, no. 29, pp. 4708–4716, Aug. 2015.
[35] A. Monti, J. Soric, M. Barbuto, D. Ramaccia, S. Velucci, F. Trotta, A. Alù, A. Toscano, and F. Bilotti, "Mantle cloaking for co-site radio-frequency antennas," *Appl. Phys. Lett.*, vol. 108, no. 11, 2016, Art. no. 113502.
[36] Z. H. Jiang and D. H. Werner, "Dispersion engineering of metasurfaces for dual-frequency quasi-three-dimensional cloaking of microwave radiators," *Opt. Exp.*, vol. 24, no. 9, p. 9629, May 2016.
[37] G. Gulati, "Novel antennas, matching circuits, and fabrication techniques at HF and microwave frequencies," M.S. thesis, Dept. Elect. Eng., Univ. Arizona, Tucson, AZ, USA, 2018.
[38] P.-Y. Chen, C. Argyropoulos, and A. Alù, "Broadening the cloaking bandwidth with non-foster metasurfaces," *Phys. Rev. Lett.*, vol. 111, no. 23, Dec. 2013, Art. no. 233001.
[39] G. Moreno, H. M. Bernety, and A. B. Yakovlev, "Reduction of mutual coupling between strip dipole antennas at terahertz frequencies with an elliptically shaped graphene monolayer," *IEEE Antennas Wireless Propag. Lett.*, vol. 15, pp. 1533–1536, Dec. 2015.
[40] P.-Y. Chen, J. C. Soric, Y. R. Padooru, H. M. Bernety, A. B. Yakovlev, and A. Alù, "Nanostructured graphene metasurface for tunable terahertz cloaking," *New J. Phys.*, vol. 15, Dec. 2013, Art. no. 123029.

[41] H. M. Bernety and A. B. Yakovlev, "Cloaking of single and multiple elliptical cylinders and strips with confocal elliptical nanostructured graphene metasurface," *J. Phys., Condens. Matter*, vol. 27, no. 18, May 2015, Art. no. 185304.
[42] H. M. Bernety, A. B. Yakovlev, H. G. Skinner, S.-Y. Suh, and A. Alù, "Decoupling and cloaking of interleaved phased antenna arrays using elliptical metasurfaces," *IEEE Trans. Antennas Propag.*, vol. 68, no. 6, pp. 4997–5002, Jun. 2020.
[43] (2015). *CST Microwave Studio CST*. [Online]. Available: http://www.cst.com
[44] D. Lee, W. Melek, and G. Shaker, "Wrapped ultra-wide band radar sensor based on resistively loaded bow-tie antenna for near zone sensing applications," *Microw. Opt. Technol. Lett.*, vol. 61, no. 4, pp. 1070–1078, Apr. 2019.
[45] D. Lee, G. Shaker, and W. Melek, "Investigation on the effects of resistive loading on wrapped bow-tie antennas," *Int. J. Microw. Wireless Technol.*, vol. 11, no. 4, pp. 390–400, May 2019.
[46] D. Lee, G. Shaker, and W. Melek, "A broadband wrapped bowtie antenna for UWB pulsed radar applications," *IEEE Trans. Antennas Propag.*, vol. 68, no. 12, pp. 7803–7812, Dec. 2020.
[47] D. M. Pozar, *Microwave Engineering*, 3rd ed. New York, NY, USA: Wiley, 2005.

DOOJIN LEE (Member, IEEE) received the Ph.D. degree in biomedical science and engineering from Gwangju Institute of Science and Technology (GIST), Gwangju, South Korea, in 2017. From 2017 to 2019, he was a Postdoctoral Fellow with the University of Waterloo (UW), Waterloo, ON, Canada. From 2019 to 2020, he was affiliated as a Postdoctoral Fellow with the Electroscience Laboratory (ESL), The Ohio State University (OSU), Columbus, OH, USA. During his second postdoctoral, he was heavily involved in several projects, such as developing a low profile of global navigation satellite system (GNSS) receiver and developing ultra-wideband non-contact ground-penetrating radar antenna. From February 2020 to September 2020, he was with the Department of Electrical Engineering, University of Mississippi (UM), Oxford, MS, USA. His research interests include ultra-wideband impulse radar sensor, impulse radar imaging, GNSS antenna receiver, and electromagnetic cloaking technique using a mantle metasurface.

ALEXANDER B. YAKOVLEV (Senior Member, IEEE) received the Ph.D. degree in radiophysics from the Institute of Radiophysics and Electronics, National Academy of Sciences, Kharkov, Ukraine, in 1992, and the Ph.D. degree in electrical engineering from the University of Wisconsin at Milwaukee, in 1997.

He joined the Department of Electrical Engineering, University of Mississippi, as an Assistant Professor, in summer of 2000, and became an Associate Professor, in 2004. Since July 2013, he has been a Full Professor of electrical engineering. He is the coauthor of the book *Operator Theory for Electromagnetics: An Introduction* (Springer, New York, NY, 2002). His research interests include mathematical methods in applied electromagnetics, homogenization theory, high-impedance surfaces for antenna applications, electromagnetic band-gap structures, metamaterial structures, wire media, graphene, cloaking, theory of leaky waves, transient fields in layered media, and catastrophe and bifurcation theories.

Dr. Yakovlev is a member of URSI Commission B. He received the Young Scientist Award at the 1992 URSI International Symposium on Electromagnetic Theory, Sydney, Australia, and the Young Scientist Award at the 1996 International Symposium on Antennas and Propagation, Chiba, Japan. He received a Junior Faculty Research Award, in 2003, and the Faculty Teaching Award in the School of Engineering at The University of Mississippi, in 2017. From 2003 to 2006, he was an Associate Editor-in-Chief of the *ACES Journal*. From 2005 to 2008, he was an Associate Editor of the IEEE TRANSACTIONS ON MICROWAVE THEORY AND TECHNIQUES. Since August 2017, he has been an Associate Editor of the IEEE ANTENNAS AND WIRELESS PROPAGATION LETTERS. Since November 2019, he has been an Associate Editor of the IEEE TRANSACTIONS ON ANTENNAS AND PROPAGATION.